Applied Physics A (2020) 126:537
https://doi.org/10.1007/s00339-020-03715-y

Applied Physics A
Materials Science & Processing

XANES investigation of novel lanthanide-doped $CuCr_{0.99}Ln_{0.01}S_2$ (Ln = La, Ce) solid solutions

E. V. Korotaev[1] · M. M. Syrokvashin[1] · I. Yu. Filatova[1] · S. V. Trubina[1] · A. D. Nikolenko[2] · D. V. Ivlyushkin[2] · P. S. Zavertkin[2] · A. V. Sotnikov[1] · V. V. Kriventsov[2,3]

Received: 3 March 2020 / Accepted: 9 June 2020 / Published online: 18 June 2020

Abstract
The study of the valence state, local environment structure and magnetic properties of novel type $CuCr_{0.99}Ln_{0.01}S_2$ (Ln = La, Ce) solid solutions was carried out using X-ray absorption spectroscopy, finite difference method simulations and static magnetic susceptibility measurements. The good agreement between experimental and calculated data indicates that cationic substitution does not lead to significant changes in the copper, chromium and sulfur local environment character and electronic density distribution. The copper atoms were found to be in Cu^+ oxidation state, the sulfur atoms—in S^{2-} oxidation state and the chromium atoms—in Cr^{3+} state. The cationic substitution of chromium by lanthanum and cerium in $CuCrS_2$ does not significantly affect the effective magnetic moment and exchange interactions character. The lanthanum-doped $CuCr_{0.99}Ln_{0.01}S_2$ solid solution demonstrates the Seebeck coefficient value 4 times greater than for $CuCrS_2$-matrix at 500 K.

Keywords XANES · Finite difference method · X-ray techniques · Simulation and modeling · Functional materials · Electronic materials · Magnetic properties · Seebeck coefficient

1 Introduction

The layered copper–chromium disulfides are promising functional materials that exhibit a wide range of functional properties for practical application: thermoelectricity [1–3], ionic conductivity [4–6] and multiferroic effects [7, 8]. The $CuCrS_2$ disulfide was recently found in the mineral composition of meteorite Uakit [9].

Cationic substitution of chromium with transition metal atoms is one of effective methods to control electric and magnetic properties in the solid solutions based on $CuCrS_2$. For example, the vanadium concentration increase in solid solutions $CuCr_{1-x}V_xS_2$ causes an increase in the ionic conductivity [4, 5] and induces a metal–insulator transition (MIT) [10–12]. The MIT is accompanied with thermoelectric properties changing [3] and arising of the colossal magnetoresistance [10, 11].

The chromium cationic substitution with the transition metals in the $CuCr_{1-x}M_xS_2$ (M = V, Mn, Fe) system is well known and investigated, but there is no information about the lanthanide-substituted copper–chromium disulfide. It should be motioned that the most promising thermoelectric properties were observed in case of low-doped solid solutions [3]. Thus, in present work the novel type of solid solutions—the lanthanum- and cerium-doped copper–chromium disulfide $CuCr_{0.99}Ln_{0.01}S_2$, was studied.

The physical properties of functional materials depend on the character of the atom distribution over crystallographic positions in the crystal lattice and the electronic density distribution features [13, 14]. Hence, the understanding of the functional properties nature requires use of the methods sensitive to the atom local environment and oxidation state. Thus, XANES (X-ray absorption near edge structure) spectroscopy was used for the electronic and spatial structure both the interpretation of the magnetic properties.

✉ E. V. Korotaev
korotaev@niic.nsc.ru

[1] Nikolaev Institute of Inorganic Chemistry, Siberian Branch of Russian Academy of Sciences, Novosibirsk, Russia

[2] Budker Institute of Nuclear Physics, Siberian Branch of Russian Academy of Sciences, Novosibirsk, Russia

[3] Boreskov Institute of Catalysis, Siberian Branch of Russian Academy of Sciences, Novosibirsk, Russia

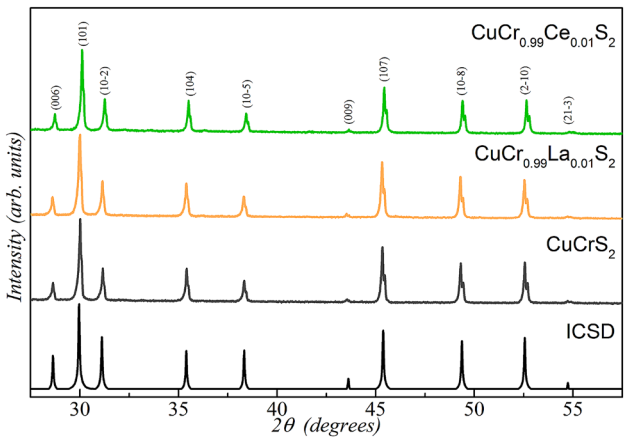

Fig. 1 Powder diffraction patterns of $CuCrS_2$ and $CuCr_{0.99}Ln_{0.01}S_2$ (Ln = La, Ce) solid solutions

Table 1 Measured unit cell parameters for $CuCrS_2$ and $CuCr_{0.99}Ln_{0.01}S_2$ (Ln = La, Ce)

Sample	*a* (Å)	*c* (Å)
$CuCrS_2$	3.480(4)	18.689(5)
$CuCr_{0.99}La_{0.01}S_2$	3.480(1)	18.693(1)
$CuCr_{0.99}Ce_{0.01}S_2$	3.480(8)	18.698(9)

2 Experimental

The samples $CuCrS_2$ and $CuCr_{0.99}Ln_{0.01}S_2$ (Ln = La, Ce) were synthesized from CuO, Cr_2O_3, La_2O_3 and CeO_2 oxides with purity of 99.99%. A mixture of oxides was placed in a horizontal boat in a quartz reactor. The air from the reaction volume was removed by argon gas flow and the decomposition products of ammonium rhodanide (NH_4SCN). The reaction mixture was heated to a temperature of 1050 °C and grounded for several times during the synthesis. The completeness of sulfidization was controlled by the samples weighing both powder X-ray diffraction (XRD). The samples under study have a rhombohedral structure (*R3m*) of α-$NaFeO_2$ (Inorganic Crystal Structure Data base (ICSD) [15]). The similarity of the diffraction patterns indicated the matrix crystal structure preservation after cationic substitution (Fig. 1). The measured unit cell parameters at room temperature are listed in Table 1. It should be noted that the lattice parameters for undoped $CuCrS_2$ matrix are in agreement with reference data [15].

X-ray absorption edges of copper atoms in the samples under study were obtained by a standard transmission mode using synchrotron radiation at VEPP-3 storage ring in Siberian Synchrotron and Terahertz Radiation Centre (Budker Institute of Nuclear Physics SB RAS, Novosibirsk). A slotted Si(111) crystal monochromator with resolution 6×10^3 was used for synchrotron radiation monochromatization [16]. X-ray absorption edges of chromium and sulfur atoms were obtained by a standard transmission mode using synchrotron radiation at VEPP-4 storage ring on the metrology station "Cosmos" in Siberian Synchrotron and Terahertz Radiation Centre (Budker Institute of Nuclear Physics SB RAS, Novosibirsk). A double crystal Si(111) monochromator with resolution ~ 1×10^4 was used for synchrotron radiation monochromatization [17].

The finite difference method for near edge structure (FDMNES software package) was used to simulate X-ray absorption near edge structure (XANES) spectra using Hedin–Lundqvist exchange and correlation potential [18, 19]. In the simulation process, the atom state with an electron vacancy (hole) on the orbital corresponding to the ground state and an additional electron on the lower unoccupied orbital was considered. The simulations for undoped disulfide matrix $CuCrS_2$ and solid solutions $CuCr_{0.99}Ln_{0.01}S_2$ (Ln = La, Ce) were performed on clusters radius of 8.5 Å consisting of 160 atoms. The simulations of the cation-substituted solid solutions were performed on the cluster with center chromium atom replaced with lanthanide atom. The unit cell parameters for quantum-chemical simulation were taken from the powder X-ray diffraction data (Table 1).

The static magnetic susceptibility measurements were carried out using the Faraday balance technique. The temperature stabilization of the samples was controlled using a Delta DTB9696 temperature controller in the temperature range of 80–740 K. The measurements were carried out in a rarefied 5 Torr helium atmosphere. The magnetic field strength was 7.3 kOe. The diamagnetic contributions into the magnetic susceptibility value were taken into account using Pascal scheme.

The Seebeck coefficient temperature dependencies were carried out in a rarefied 5 Torr helium atmosphere on the cylindrical compressed (~ 70 MPa) samples placed between two copper contact pads. The samples were compressed in vacuum at 650 °C. The estimated sample density was ~ 4.1 g/cm^3. The 10 °C temperature gradient between the copper pads was maintained by Thermodat-13K5 temperature controller. The thermoelectric power occurring between the pads was measured using digital voltmeter Belvar V7-53.

3 Results and discussion

X-ray absorption near-edge structure (XANES) spectroscopy is a well-established technique providing data on the electronic and spatial structure. The absorption edge energy corresponds to the core-level energy characterizing the elements oxidation state. The spectral shape in the near-edge

region provides information about the electronic properties and the local environment of the absorbing atom [20].

3.1 Copper K-edges

The copper K-edges of undoped matrix $CuCrS_2$ and $CuCr_{0.99}Ln_{0.01}S_2$ (Ln = La, Ce) solid solutions are shown in Fig. 2. The similarity of the K-edges before and after cationic substitution indicates that the copper local environment surrounding character is preserved after cationic substitution. The simulated XANES spectra (Fig. 2) are in good agreement with experimental data. It should be noted that pre-edge structure in case of the experimental edges was not resolved well enough as in simulated spectra. The mismatch between theoretical and experimental results could be due to the chemical bonding description in terms of the local density approximation (LDA). The LDA method considers the inhomogeneous electron density as being locally homogeneous and uses the exchange–correlation hole known for the homogeneous system. Thus, the features located in the pre-edge region (A_0) sensitive to the bond hybridization near Fermi level (as well as local environment character) could be overestimated [21, 22].

The line-shape analysis of experimental and simulated Cu K-edges has shown the *B* feature intensity increase after cationic substitution. The energy position (8980.7 eV) of the experimental copper K-edge inflection point of the pre-edge shoulder does not change after cationic substitution. This fact indicates that cationic substitution does not significantly affect the electronic density for copper atoms. It was previously shown that the oxidation state in undoped disulfide matrix could be described as follows $Cu^{+}Cr^{3+}(S^{2-})_2$ [8, 13, 23]. Therefore, the copper oxidation state (Cu^{+}) remains the same as in the initial matrix.

3.2 Chromium K-edges

The chromium K-edges of $CuCrS_2$ and $CuCr_{0.99}Ln_{0.01}S_2$ (Ln = La, Ce) are shown in Fig. 3. The fine structure (features A_0–*E*) similarity indicates the similarity of the local environment character of chromium atoms after cationic substitution. The experimental spectra line-shape is well agreed with simulated spectra. The lower intensity of *D* feature in comparison with those in the experimental K-edges could be due to the spectra convolution procedure used in the FDMNES software package. The high-energy feature *E*

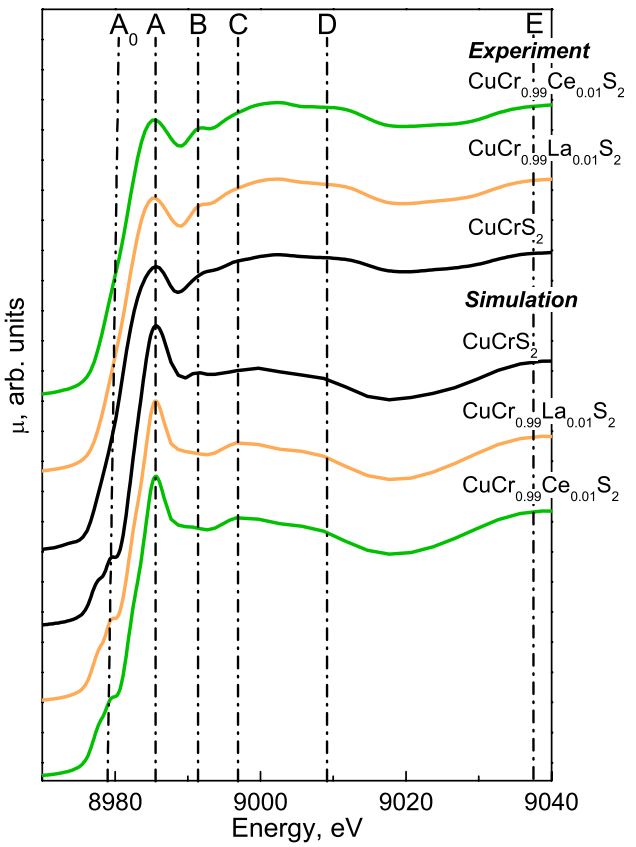

Fig. 2 Experimental and simulated CuK-edges in $CuCrS_2$ and $CuCr_{0.99}Ln_{0.01}S_2$ (Ln = La, Ce) solid solutions

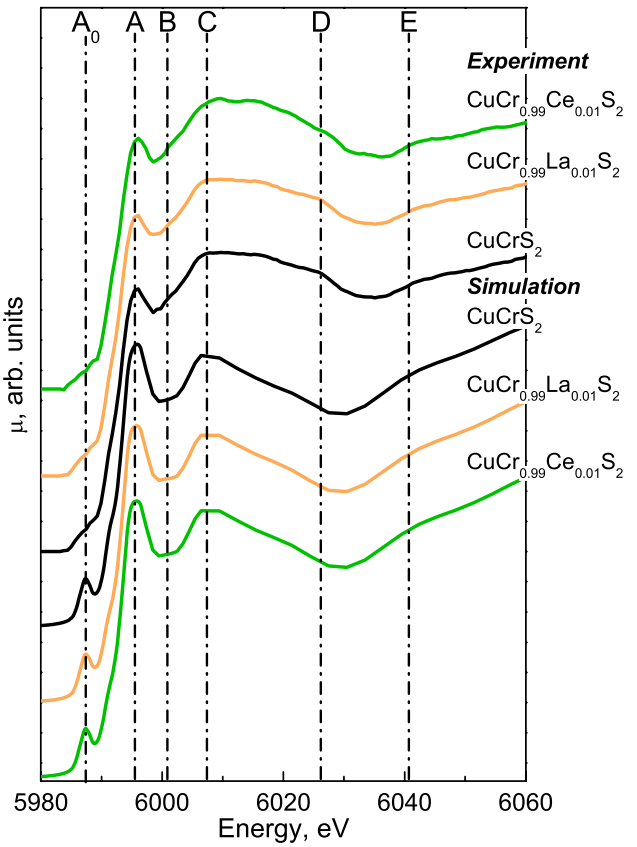

Fig. 3 Experimental and simulated CrK-edges in $CuCrS_2$ and $CuCr_{0.99}Ln_{0.01}S_2$ (Ln = La, Ce) solid solutions

could be related to the extended X-ray absorption fine structure (EXAFS) [24]. The calculations in the EXAFS region require a different approach taking into account the interference between the outgoing photoelectron wave functions from the absorbing atoms and the returning wave functions backscattered from atoms in the surrounding region [25–27]. The energy position (5993.3 eV) of the experimental chromium K-edge inflection point of the pre-edge shoulder does not change after cationic substitution. Thus, one can conclude that cationic substitution with lanthanides does not significantly affect the electronic density for chromium atoms. Therefore, the chromium oxidation state (Cr^{3+}) in lanthanide-doped solid solutions remains the same as in the initial matrix.

3.3 Sulfur K-edges

The sulfur K-edges of $CuCrS_2$ and $CuCr_{0.99}Ln_{0.01}S_2$ (Ln = La, Ce) are shown in Fig. 4. The similarity of the experimental sulfur K-edges for $CuCrS_2$ and doped solid solutions indicates the sulfur local environment character preservation. The fine structure of the simulated spectra is well agreed with experimental data. However, the pre-edge features A_1 and A_2 have "*inverse*" ratio in comparison with those for the experimental spectra. It could be due to LDA method limitations concerning chemical bonding description that was mentioned above (see paragraph 3.1). The cationic substitution of $CuCrS_2$ with lanthanum and cerium led to the intensity increase in *B, D* and *E* features. This trend is in good agreement with proposed substitution model both in the experiment and simulated spectra. The energy position (2469.7 eV) of A_1 feature does not change after cationic substitution and corresponds to S^{2-} oxidation state. The absent of energy position shifts of sulfur K-edges indicates that cationic substitution does not significantly affect the electronic density of sulfur atoms.

3.4 Simulation for lanthanide L_3-edges

The simulated L_3-edge for lanthanum and cerium in $CuCr_{0.99}Ln_{0.01}S_2$ (Ln = La, Ce) is shown in Fig. 5. The local environment in case of La- and Ce-doped solid solutions is the same. Hence, one could expect the lanthanide L_3-edges features similarity. This statement is in good agreement with simulation results (Fig. 5). It should be mentioned that lanthanum and cerium L_3-edges are plotted with the respect to the edge energies (E_{edge}). Thus, one can note that the energy position of the pre-edge feature A, the low-energy features *B–D* both the high-energy feature *E* are the same for La- and Ce-doped solid solutions. The absent of the significant energy position shifts of the X-ray absorption edges discussed above (see Sects. 3.1–3.3) and

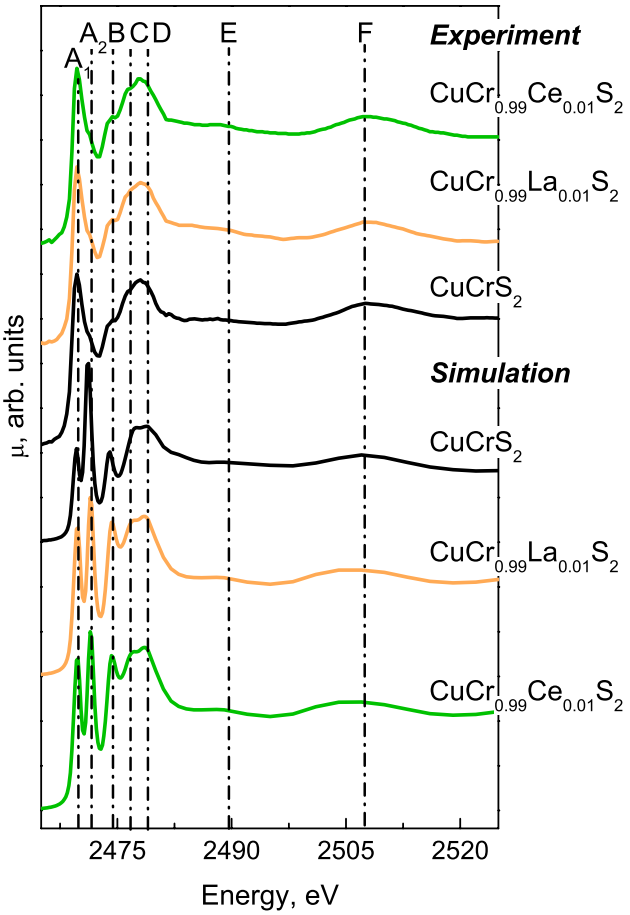

Fig. 4 Experimental and simulated S K-edges in $CuCrS_2$ and $CuCr_{0.99}Ln_{0.01}S_2$ (Ln = La, Ce) solid solutions

taking into account the charge balance allow one to conclude that lanthanide atoms should be in Ln^{3+} oxidation state.

3.5 Magnetic susceptibility

The molar magnetic susceptibility temperature dependencies for $CuCrS_2$ and $CuCr_{0.99}Ln_{0.01}S_2$ (Ln = La, Ce) are shown in Fig. 6 (the filled symbols). The linear dependence of the invert magnetic susceptibility (Fig. 6, the empty symbols) allows one to approximate obtained dependencies using Curie–Weiss law [28, 29]:

$$\chi(T) = \frac{C}{T-\theta} = \frac{N_A \mu_B^2}{3k(T-\theta)}\mu_{eff}^2, \quad (1)$$

where T is temperature, k is the Boltzmann constant, N_A is the Avogadro number, μ_B is the Bohr magneton, μ_{eff} is the effective magnetic moment and θ is the paramagnetic Curie temperature:

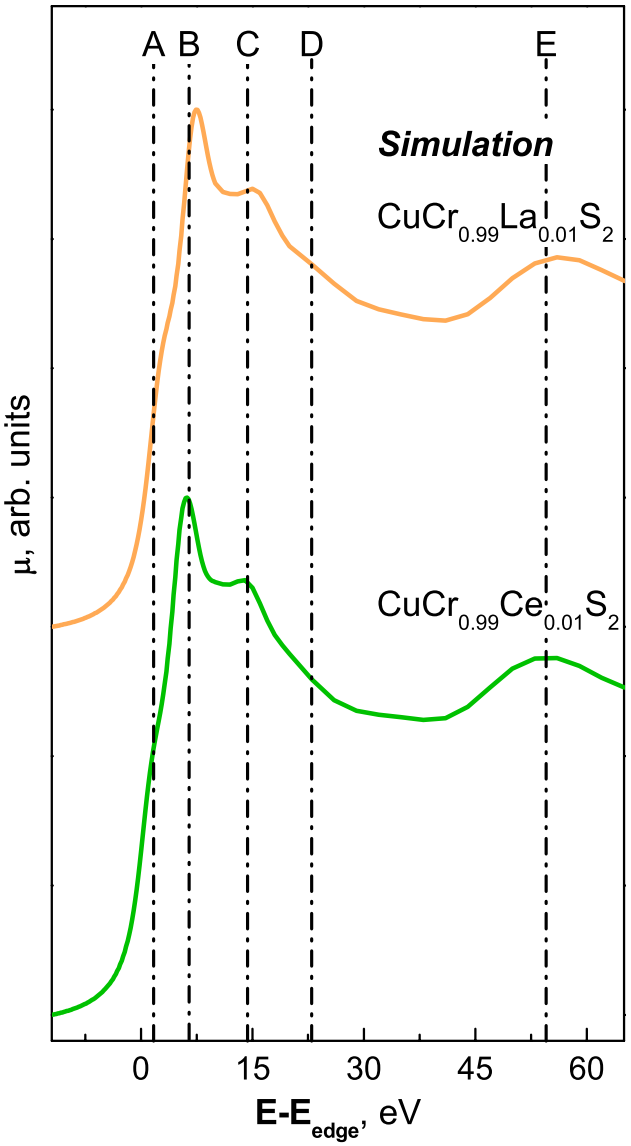

Fig. 5 Simulated Ln L_3-edges in $CuCr_{0.99}Ln_{0.01}S_2$ (Ln = La, Ce) solid solutions

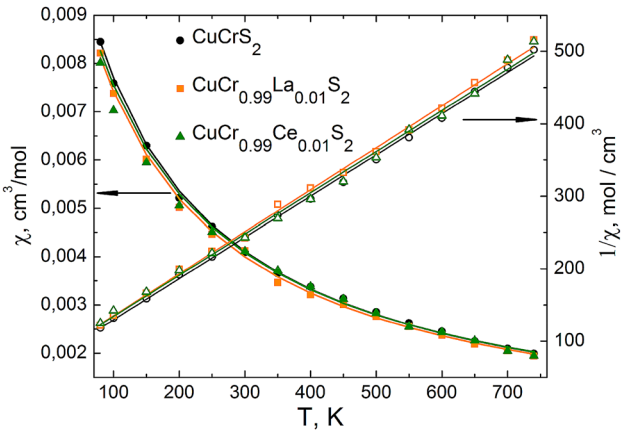

Fig. 6 Static magnetic susceptibility measurements for $CuCrS_2$ and $CuCr_{0.99}Ln_{0.01}S_2$ (Ln = La, Ce) solid solutions: $\chi(T)$ (filed symbols) and $1/\chi(T)$ (empty symbols)

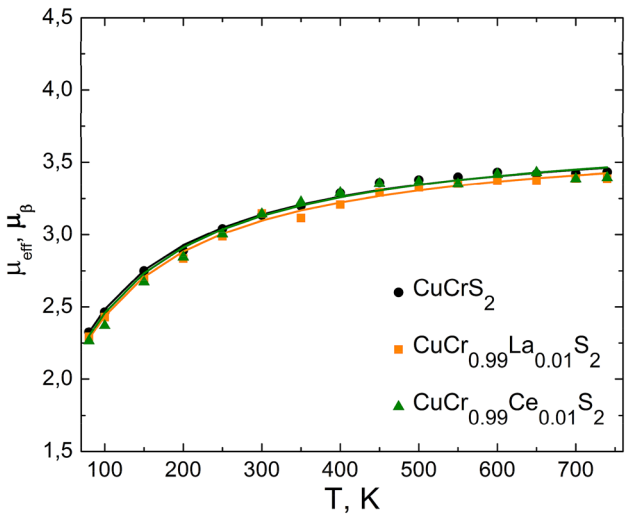

Fig. 7 Effective magnetic moment for $CuCrS_2$ and $CuCr_{0.99}Ln_{0.01}S_2$ (Ln = La, Ce)

$$\theta = \frac{2S(S+1)}{3k} \sum z_i J_i, \tag{2}$$

where S is the spin, z_i is the magnetic coordination number, J_i is the exchange interaction between magnetic centers, i is the magnetic center number.

The approximation results are shown in Figs. 6 and 7 by the solid lines. The $\mu_{eff} = 3.75 \pm 0.03\ \mu_B$ for $CuCrS_2$ is in good agreement with the $Cu^{+}Cr^{3+}(S^{2-})_2$ distribution and corresponds to Cr^{3+} oxidation state ($\mu_{theor.} = 3.87\ \mu_B$). The cationic substitution does not significantly affect the μ_{eff} value for $CuCr_{0.99}La_{0.01}S_2$ ($\mu_{eff} = 3.71 \pm 0.03\ \mu_B$) and $CuCr_{0.99}Ce_{0.01}S_2$ ($\mu_{eff} = 3.77 \pm 0.05\ \mu_B$) in comparison with those for $CuCrS_2$. Thus, one can conclude that cationic substitution does not affect the chromium and copper oxidation state. It should be emphasized that this fact is in good agreement with XANES data discussed above.

The paramagnetic Curie temperature analysis has shown that the mean exchange interaction integrals $\Sigma z_i J_i$ are negative. That fact corresponds to the prevalence of antiferromagnetic exchange interactions in the compounds studied. The cationic substitution does not significantly affect the paramagnetic Curie temperature value ($\theta = -125 \pm 6$ K ($CuCrS_2$), -133 ± 4 K ($CuCr_{0.99}La_{0.01}S_2$) and -135 ± 5 K ($CuCr_{0.99}La_{0.01}S_2$)). The θ value for $CuCrS_2$ is in good agreement with data reported in [7, 13, 23 and 24]. It should be also noted that that the effective magnetic moment temperature dependence (Fig. 7) character is typical for antiferromagnetic compounds [28, 29].

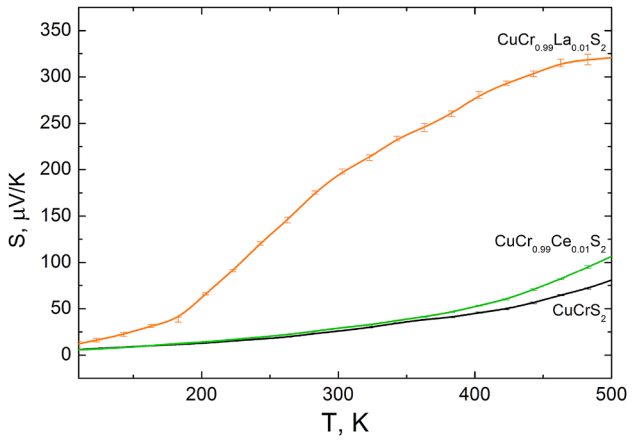

Fig. 8 Seebeck coefficient temperature dependence for $CuCrS_2$ and $CuCr_{0.99}Ln_{0.01}S_2$ (Ln = La, Ce) solid solutions

The μ_{eff} value increases as a function of temperature in $CuCrS_2$ and $CuCr_{0.99}Ln_{0.01}S_2$ (Ln = La, Ce). The antiferromagnetic ordering of magnetic moments in the case of $CuCrS_2$-matrix at temperatures below the Neel temperature ($T_N \approx 40$ K) was shown in [7, 13, 23 and 24]. In the temperature range above T_N, the inverse magnetic susceptibility of $CuCrS_2$ was found to be linear and could be described in terms of Curie–Weiss law. In the vanadium-doped solid solutions $CuCr_{1-x}V_xS_2$ ($x < 0.2$), the antiferromagnetic ordering characteristic to the CuCrS2-matrix is preserved [23]. Thus, one can conclude that antiferromagnetic ordering at low temperature range for lanthanide-doped solid solutions $CuCr_{0.99}Ln_{0.01}S_2$ is preserved.

3.6 Seebeck coefficient

The temperature dependences of the Seebeck coefficient (S) for lanthanide-doped solid solutions $CuCr_{0.99}Ln_{0.01}S_2$ and $CuCrS_2$-matrix are shown in Fig. 8. The positive sign of S indicates *p*-type conduction in the temperature range of 100 to 500 K. The largest S values over investigated temperature range were observed for $CuCr_{0.99}La_{0.01}S_2$ (the maximum value is ~ 320 μV/K at 500 K). The Seebeck coefficient increases in the row $CuCrS_2 \rightarrow CuCr_{0.99}Ce_{0.01}S_2 \rightarrow CuCr_{0.99}La_{0.01}S_2$. The increase in S could be due to the metal-isolator transition in the cation-substituted solid solutions [3]. The significant increase in S in $CuCr_{0.99}La_{0.01}S_2$ could be associated with the electronic structure features of lanthanum, since Ln^{3+} has an empty 4*f*-shell. The replacing of chromium 3d-states with empty lanthanum 4f-states leads to the electronic density decrease in the valence band region. Thus, the Seebeck coefficient value in the lanthanide-doped solid solution increases in comparison with those for $CuCrS_2$-matrix.

4 Conclusion

The comprehensive study of the lanthanide-doped solid solutions $CuCr_{0.99}Ln_{0.01}S_2$ (Ln = La, Ce) using X-ray absorption spectroscopy and static magnetochemistry was carried out.

The local atomic environment in the lanthanide-doped solid solutions $CuCr_{0.99}Ln_{0.01}S_2$ remains unaffected after cationic substitution. The cationic substitution of chromium was confirmed by the changes observed in the K-edges fine structure features intensity. The similarity of the simulated and experimental data validates the proposed model of the cationic substitution.

The copper atoms were found to be Cu^+, the chromium atoms—Cr^{3+} and the sulfur atoms S^{2-} oxidation state. The lanthanide atoms were found to be Ln^{3+} due to the absence of the significant changes of the X-ray absorption K-edges both the charge balance.

The cationic substitution for $CuCr_{0.99}Ln_{0.01}S_2$ (Ln = La, Ce) does not significantly affect magnetic properties. However, there is an affect on the Seebeck coefficient value for $CuCr_{0.99}Ln_{0.01}S_2$ (Ln = La, Ce) in comparison with those for $CuCrS_2$-matrix was observed. The lanthanum-doped solid solution has the largest Seebeck coefficient value (4 times greater than for $CuCrS_2$-matrix at 500 K). This could be due to the electronic structure features of lanthanum, since Ln^{3+} has an empty 4*f*-shell.

Acknowledgements The study was carried out with a funding from the Russian Science Foundation (Project No. 19-73-10073). The X-ray absorption spectra were measured using the shared research center SSTRC on the basis of the Novosibirsk VEPP-4 - VEPP-2000 complex at BINP SB RAS, using equipment supported by Project RFMEFI62119X0022.

References

1. Y.-X. Chen, B.-P. Zhang, Z.-H. Ge, P.-P. Shang, Preparation and thermoelectric properties of ternary superionic conductor $CuCrS_2$. J. Solid State Chem. **186**, 109–115 (2012). https://doi.org/10.1016/j.jssc.2011.11.040
2. A. Kaltzoglou, P. Vaqueiro, T. Barbier, E. Guilmeau, A. Powell, Ordered-defect sulfides as thermoelectric materials. J. Electron. Mater. **43**, 2029–2034 (2014). https://doi.org/10.1007/s11664-013-2941-0
3. E.V. Korotaev, M.M. Syrokvashin, IYu. Filatova, K.G. Pelmenev, V.V. Zvereva, N.N. Peregudova, J. Electron. Mater. **47**, 3392–3397 (2018). https://doi.org/10.1007/s11664-018-6230-9
4. R.F. Al'mukhametov, R.A. Yakshibaev, E.V. Gabitov, Phys. Solid State **41**, 1327–1328 (1999). https://doi.org/10.1134/1.1130992
5. R.F. Al'mukhametov, R.A. Yakshibaev, E.V. Gabitov, A.R. Abdullin, R.M. Kutusheva, Phys. Stat. Sol. B **236**, 29–33 (2003). https://doi.org/10.1002/pssb.200301413

6. G.R. Akmanova, A.D. Davleshina, Lett. Mater. **3**, 76–78 (2013)
7. A. Karmakar, K. Dey, S. Chatterjee, S. Majumdar, S. Giri, Appl. Phys. Lett. **104**, 052906 (2014). https://doi.org/10.1063/1.4863937
8. F.M.R. Engelsman, G.A. Wiegers, F. Jellinek, B. van Laar, J. Solid State Chem. **6**, 574–582 (1973). https://doi.org/10.1016/S0022-4596(73)80018-0
9. R. Miyawaki, F. Hatert, M. Pasero, S. Mills, Miner. Mag. **83**, 887–893 (2019). https://doi.org/10.1180/mgm.2019.73
10. G.M. Abramova, G.A. Petrakovskii, Low Temp. Phys. **32**, 725–734 (2006). https://doi.org/10.1063/1.2219495
11. G. Abramova, A. Pankrats, G. Petrakovskii, J.C.E. Rasch, M. Boehm, A. Vorotynov, V. Tugarinov, R. Szumszak, A. Bovina, V. Vasil'ev, J. Appl. Phys. **107**, 931 (2010)
12. N. Tsujii, H. Kitazawa, G. Kido, Phys. Stat. Sol. (C) **3**, 4417–4418 (2006). https://doi.org/10.1002/pssc.200669659
13. N. Le Nagard, G. Collin, O. Gorochov, Mater. Res. Bull. **14**, 1411–1417 (1979). https://doi.org/10.1016/0025-5408(79)90083-7
14. I.G. Vasileva, V.V. Kriventsov, J. Synch. Investig. **4**, 640–644 (2010). https://doi.org/10.1134/S1027451010040178
15. Inorganic crystal structure database. Version 2.1.0/FIZ Karlsruhe, Germany
16. Experimental station "EXAFS spectroscopy". http://ssrc.inp.nsk.su/CKP/eng/stations/passport/8/. Accessed 18 June 2018
17. P.S. Zavertkin, D.V. Ivlyushkin, M.R. Mashkovtsev, A.D. Nikolenko, S.A. Sutormina, N.I. Chkhalo, Optoelectron. Instrum. Proc. **55**, 107–114 (2019). https://doi.org/10.3103/s8756699019020018
18. S.A. Guda, A.A. Guda, M.A. Soldatov, K.A. Lomachenko, A.L. Bugaev, C. Lamberti, W. Gawelda, C. Bressler, G. Smolentsev, A.V. Soldatov, Y. Joly, J. Chem. Theory Comput. **11**, 4512–4521 (2015). https://doi.org/10.1021/acs.jctc.5b00327
19. Y. Joly, Phys. Rev. B **63**, 125120–125129 (2001). https://doi.org/10.1103/PhysRevB.63.125120
20. G.S. Henderson, F.M. de Groot, B.J. Moulton, Rev. Miner. Geochem. **78**, 75–138 (2014). https://doi.org/10.2138/rmg.2014.78.3
21. J.W. Niemantsverdriet, *Spectroscopy in Catalysis: An Introduction, 3rd, Completely Revised and Enlarged Edition* (Wiley-VCH Verlag GmbH & Co. KGaA, Weinheim, 2007), p. 326
22. G.J. Schmitz, U. Prahl, *Handbook of Software Solutions for ICME* (Wiley-VCH Verlag GmbH & Co. KGaA, Weinheim, 2017), p. 595
23. N. Tsujii, H. Kitazawa, Substitution effect on the two-dimensional triangular-lattice system $CuCrS_2$. J. Phys. Condens. Matter **19**, 145245 (2007). https://doi.org/10.1088/0953-8984/19/14/145245
24. M.M. Syrokvashin, E.V. Korotaev, IYu. Filatova et al., Spectrochim. Acta Part A Mol. Biomol. Spectrosc. **205**, 593–596 (2018). https://doi.org/10.1016/j.saa.2018.07.053
25. O. Bunau, Y. Joly, J. Phys. Condens. Matter **21**, 345501 (2009). https://doi.org/10.1088/0953-8984/21/34/345501
26. J.D. Bourke, C.T. Chantler, Phys. Rev. Lett. **104**, 206601 (2010). https://doi.org/10.1103/PhysRevLett.104.206601
27. J.D. Bourke, C.T. Chantler, Y. Joly, J. Synchrotron Rad. **23**, 551–559 (2016). https://doi.org/10.1107/S1600577516001193
28. S. Blundell, *Magnetism in Condensed Matter* (Oxford University Press, New York, 2001)
29. P. Selwood, *Magnetochemistry*, 2nd edn. (Interscience Publishers, New York, 1956)